The Deformation and Adhesion of Randomly Rough and Patterned Surfaces

Marcel Benz,[†] Kenneth J. Rosenberg,[‡] Edward J. Kramer,[†] and Jacob N. Israelachvili*[,†]

Department of Chemical Engineering, Materials Department, and Materials Research Laboratory, University of California, Santa Barbara, California 93106, and Department of Physics, University of California, Santa Barbara, California 93106

Received: January 15, 2006; In Final Form: April 6, 2006

Using a surface forces apparatus (SFA) and an atomic force microscope (AFM) we have studied the effects of surface roughness (root-mean-square (RMS) roughness between 0.3 and 220 nm) on the "contact mechanics", which describes the deformations and loading and unloading adhesion forces, of various polymeric surfaces. For randomly rough, moderately stiff, elastomeric surfaces, the force−distance curves on approach and separation are nearly reversible and almost perfectly exponentially repulsive, with an adhesion on separation that decreases only slightly with increasing RMS. Additionally, the magnitude of the preload force is seen to play a large role in determining the measured adhesion. The exponential repulsion likely arises from the local compressions (fine-grained nano- or submicron-scale deformations) of the surface asperities. The resulting characteristic decay lengths of the repulsion scale with the RMS roughness and correlate very well with a simple finite element method (FEM) analysis based on actual AFM topographical images of the surfaces. For "patterned" surfaces, with a nonrandom terraced structure, no similar exponential repulsion is observed, suggesting that asperity height variability or random roughness is required for the exponential behavior. However, the adhesion force or energy between two "patterned" surfaces fell off dramatically and roughly exponentially as the RMS increased, likely owing to a significant decrease in the contact area which in turn determines their adhesion. For both types of rough surfaces, random and patterned, the coarse-grained (global, meso- or macroscopic) deformations of the initially curved surfaces appear to be Hertzian.

Introduction

Surface roughness affects many physical and mechanical properties of surfaces and materials at length scales from the macroscopic to the nanoscopic. This includes their adhesion, tribology (friction and wear), local deformations, yield stresses, the nucleation of cracks, and failure mechanisms.[1,2] Roughness also has a large effect on the interactions of granular materials and colloidal particles in solution.[3,4] Whereas "ideal" surfaces, for which most theories have been developed, are molecularly smooth, most "real" surfaces display roughness over a wide range of length scales or RMS values. There is, as of yet, no generally accepted way of defining the complex roughness or topography of a non self-affine surface.[5,6]

For this reason, the role of surface roughness in determining adhesion and/or friction has been difficult to quantify. These properties also depend on a number of additional surface and bulk material properties, both physical and chemical. For example, a soft, ductile material or viscoelastic polymer behaves very differently from an elastomeric polymer, even if their RMS roughness and thermodynamic surface energies γ are the same. In a number of currently evolving technological areas, especially those involving micro-electro−mechanical systems (MEMS)[7,8] and hard drives,[9,10] as these devices become smaller, surface roughness plays an increasingly important role. Recent experiments[11] and computer simulations[12,13] have shown that even atomic scale roughness, i.e., at the sub-nanometer scale, let alone at the nanometer scale and above, can drastically change contact areas and surface stresses, especially shear stresses. In many cases, to design and create surfaces with desirable adhesion or "stickiness" requires the ability to control their roughness and texture. The question addressed in this paper is "how does surface roughness affect adhesion?" The question addressing friction will be addressed in a separate paper.

The most common approach to measuring roughness and its effect on surface forces is to employ an atomic force microscope (AFM) cantilever with a sharp tip or colloidal particle at its end.[14,15] The work described here uses a surface force apparatus (SFA) to measure the forces between two macroscopically curved surfaces and AFM to image these surfaces. The SFA has the advantage in that absolute normal distances (surface separations) can be measured at the ångstrom level, as can the lateral surface deformations and contact areas, although only at the micron-scale. Vanderlick and co-workers[16,17] used an SFA to measure the adhesion and deformation of rough gold and silver surfaces when pressed against a surface of molecularly smooth mica. The ductile asperities on these surfaces were a few nanometers at most and deformed plastically under the action of the strong van der Waals forces between metal surfaces. Similar work by Alcantar et al.[18] looked at symmetric nanoparticle-coated gold surfaces that coalesced abruptly with each other when gently pressed together. For elastic surfaces, Kim and Russell[19] measured the adhesion energy between a PDMS elastomer and a polystyrene/poly(methyl methacrylate) diblock copolymer at different roughnesses. Interestingly, they found that the highest adhesion force occurred at some intermediate roughness of the diblock.

Here, we have focused on two different classes of rough surfaces: patterned (or quasi-ordered) and random. Using a SFA,

* To whom correspondence should be addressed. Email: jacob@engineering.ucsb.edu.
[†] Department of Chemical Engineering.
[‡] Department of Physics.

10.1021/jp0602880 CCC: $33.50
Published on Web 05/26/2006

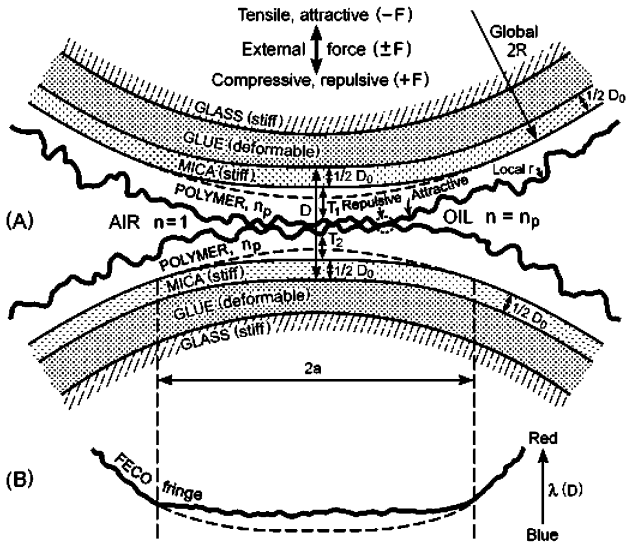

Figure 1. Schematic of rough surfaces in contact. The polymer layers were either P(VDF−TrFE) for the randomly rough surfaces or PS−PVP for the patterned surfaces.

the forces during compression and separation between two crossed cylindrical surfaces were measured. The work extends some earlier SFA measurements[20−22] of the repulsive forces between various rough and particle-covered surfaces to a more systematic study of both the repulsive and attractive (adhesion) forces between surfaces with varying, well-characterized roughness. To do this, we have applied some recently developed techniques for preparing such surfaces and have used AFM imaging of the surfaces to obtain their RMS roughness and, more generally, their 3D asperity distributions or topographies. We find what appear to be some universal force laws and scaling relations between roughness and (1) the adhesion of elastic polymer surfaces and (2) the repulsive forces at distances closer than the adhesive energy minima.

Experimental Techniques

Surface Forces Apparatus (SFA). Using a SFA III,[23] forces were measured as previously described between two initially curved surfaces of radius $R \approx 2$ cm in the crossed-cylinder geometry, which is locally equivalent to a sphere of radius R on a flat surface or to two spheres each of radius $2R$.[26] The geometry is shown schematically in Figure 1. Only normal forces (adhesion and repulsion) are reported in this study. The polymer surfaces were prepared as described below, and all measurements were made at 23 ± 0.1 °C.

Some experiments were conducted with the surfaces in an inert atmosphere of dry nitrogen gas (the SFA chamber is hermetically sealed), whereas others were carried out with lubricant oils between the surfaces. The oils were inert "immersion oils" or "refractive index liquids" of aliphatic and alicyclic hydrocarbons from SPI Supplies (West Chester, PA). For each of the two polymer systems studied, the oil was chosen to match the refractive index of the polymer, viz. $n = 1.59$ for the PS−PVP diblock (patterned surfaces), and $n = 1.42$ for the P(VDF−TrFE) copolymer (randomly rough surfaces). The refractive index liquids did not swell or dissolve the polymers.

Optical Visualization of Interacting Surfaces Using Feco Fringes. Visualization of the surface geometry employed multiple beam interferometry (MBI), which produces so-called fringes of equal chromatic order (FECO). This technique uses white light that is passed perpendicularly through the polymer-coated mica sheets. The mica sheets have highly reflecting silver layers on their backsides, which act as semireflecting mirrors. Each wavelength of the white light undergoes multiple reflections between these mirrors before leaving the interferometer. The emerging beam, which consists of a series of sharp fringes that have undergone constructive interference, is then focused onto the slit of a grating spectrometer, which splits the beam into its different wavelength components (the FECO). Through analysis of the positions and shapes of the emerging FECO fringes, one obtains quantitative information on the following (cf. Figure 1): the film thickness and separation between the two surfaces at different locations in the $x-y$ plane (the normal resolution in the z-direction is ∼0.1−0.2 nm), the global and local geometry, and surface radii R and r (the lateral resolution in the $x-y$ plane is ∼1 μm), and the mean index of refraction n_m of the intervening medium. By compressing the two initially curved surfaces together, one is further able to measure the projected (global) contact radius a and projected area $A = \pi a^2$ of the elastically or plastically flattened contact region.

Calculation of Force−Distance Profiles and Adhesion Forces. It is straightforward to calculate the force−distance profiles, $F(D)$, on approach (compressive loading) and separation (unloading) and, under high loads, the mean pressure $P = F/A = F/\pi a^2$ between the two flattened surfaces. The elastic deformation of adhering surfaces is analyzed by the Johnson−Kendall−Roberts (JKR) theory.[27] It allows for the estimation of the adhesion energy (surface energy) from the measured adhesion or "pull-off" force F_{ad} needed to separate the adhering surfaces. For two crossed-cylindrical surfaces F_{ad} is given by[28]

$$F_{ad} = 3\pi R\gamma = \frac{3}{2}\pi R W_0 \qquad (1)$$

where the surface or interfacial energy γ is by definition half of the thermodynamic adhesion energy or work of adhesion, W_0. In the case of adhesion hysteresis, the surface energy for "advancing/approaching" surfaces on loading, W_A, is lower than for "retracting/receding" surfaces on unloading, W_R, and both can be higher or lower than W_0. W_A and W_R can be extracted by measuring the apparent (macroscopic) contact radius a as a function of the applied load F at increasing and decreasing loads, respectively, and fitting the data to the JKR equation.[25] W_R can also be obtained from the measured pull-off force using eq 1. In our experiments, the rates of loading and unloading were the same for all samples ($dF/dt = \pm 10^{-4}$ N/s), and the surfaces were kept in compressive contact at the highest applied loads, F_{max}, for one minute before they were separated.

Polymers Used. There are a number of materials whose surfaces are naturally rough. For example, thin films of deposited gold or silver are known to have nanometer-sized asperities.[17] However, these ductile noble metal surfaces, when compressed in the SFA, result in irreversible plastic deformations[16] and ultimate coalescence (cold welding) of the asperities.[18] In contrast, hard, brittle surfaces, e.g., of ceramic materials, are difficult to process, have a limited range of mechanical properties (e.g., no viscoelasticity), and their high-energy surfaces are chemically reactive and prone to picking up organic impurities from the atmosphere. The roughness we desired was to be relevant to many "engineering" applications (10^0 nm < RMS < 10^2 nm), and we further looked for compounds that could be easily deposited (spin-cast, solution-cast, or LB-deposited) as a film on mica to produce elastic or viscoelastic films.

Two different polymers were chosen, each producing a qualitatively different surface morphology. The first, the diblock copolymer poly(styrene-b-2-vinylpyridine), PS−PVP, has an

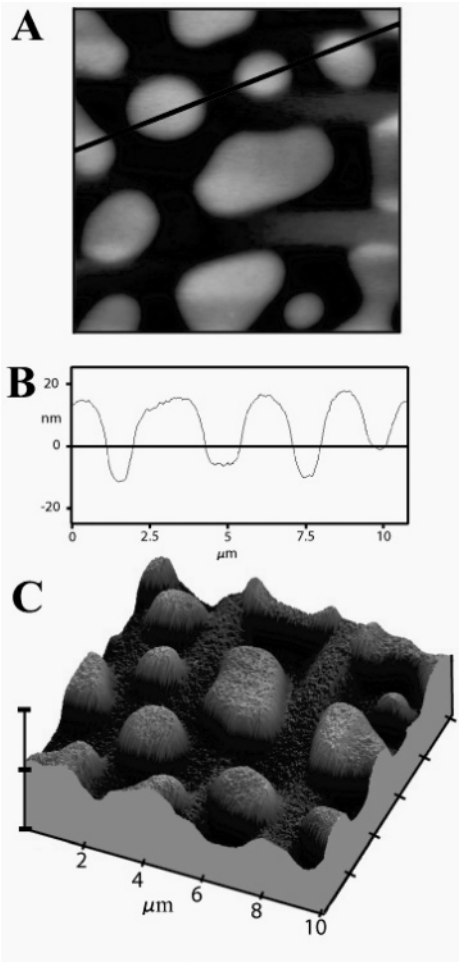

Figure 2. (A) AFM image of a "patterned" PS−PVP diblock copolymer surface showing island formation after annealing of the 52-nm thick polymer film ($\sigma = 6.0 \pm 0.5$ nm). (B) Cross section through the image showing that all asperities have very similar heights. (C) Same image as in (A) but viewed at an angle. In contrast to the randomly rough surfaces of P(VDF−TrFE) for which $T_g = -28$ °C, for PS−PVP $T_g = +100$ °C, i.e., the "patterned" surfaces were also much stiffer than the "rough" surfaces, and their chains were much less mobile.

inherently asymmetric molecular structure.[29,30] The volume fraction of the PVP used was 0.13, and the number average molecular weight was $M_n = 7 \times 10^4$ with a polydispersity of less than 1.12 and a glass transition temperature of $T_g \approx 100$ °C. After spin casting a polymer film and annealing it above T_g, this asymmetric block copolymer forms layered spherical domains that propagate from the underlying substrate (Figure 2). Depending on the initial thickness of the film, these layered structures can resemble islands or holes at the free interface. Thus, different surface topographies could be produced by varying the polymer film thickness, annealing time, and annealing temperature. The elastic modulus of PS−PVP is expected to be similar to that of bulk PS (3 GPa) because the PVP only constitutes 13% of the total composition. This copolymer was chosen to produce our "patterned" surfaces (Figure 2).

The polymer chosen to produce films with varying random surface roughness was poly(vinylidene fluoride−trifluoroethylene), P(VDF−TrFE), from KTECH Corporation, (Albuquerque, NM). The volume fraction of TrFE was 0.35 and the molecular weights of the P(VDF−TrFE) copolymer were $M_w \approx 5 \times 10^6$ and $M_n \approx 7 \times 10^4$ g/mol. The T_g of the copolymer is about −28 °C, and its elastic modulus is 1.8 GPa. This semicrystalline polymer was chosen because the thin film surface morphology of P(VDF−TrFE) as well as the processing parameters that determine the random surface roughness have been well-described.[31−33] Briefly, the heterogeneous surface morphology of the polymer can be altered simply by varying any of the following parameters: the temperature of the polymer solution used to dissolve the P(VDF−TrFE), the solvent composition, the rate of evaporation, and the relative humidity when deposited onto a substrate. P(VDF−TrFE) rather than PVDF was used in this study because of the copolymer's increased solubility in a 9:1 acetone/dimethylformamide (DMF) solvent and simpler crystallographic properties (only one crystalline phase as opposed to three forms for PVDF). The relative humidity at which the copolymer film was deposited and dried turned out to be the most important parameter for determining the film topography.

Surface Preparation. Once the mica sheets were glued onto the glass disks, the untreated surfaces were installed into the SFA chamber to measure (calibrate) the separation $D = 0$, which corresponded to mica−mica contact (Figure 1).[34] The surfaces were then removed from the SFA chamber for the polymer layer depositions.

The PS−PVP diblock layers were deposited on each mica surface by spin coating from a 1.5 wt % solution in toluene. The thickness of the spin cast film was controlled by modifying the spin speed. To obtain a quick preliminary estimate of the film thickness, the polymer film was first spin cast on silicon wafer substrates. Ellipsometry of these samples was used to determine the proper rotation speed to generate a ∼52−55-nm thick film on mica. After depositing on both mica surfaces, they were immediately transferred into a vacuum oven and annealed at $\sim 10^{-7}$ Torr for different times and temperatures depending on the roughness desired. Typically, temperatures around 180 °C for 1−2 h were sufficient to produce these patterned structures. The polymer-coated mica surfaces were then cooled to room temperature and reinserted into the SFA.

For the P(VDF−TrFE) copolymer layers, 5.0 wt % P(VDF−TrFE) was dissolved in a 9:1 acetone/dimethylformamide (DMF) solvent at room temperature. Both solvents were from Sigma, St. Louis, MO. The polymer film deposition was again done by spin coating onto the mica surfaces. The relative humidity during the solvent evaporation, which determines the heterogeneous surface morphology of the film, was altered by an infrared lamp positioned at different heights above the spin coater. The light emission changed the local temperature, which in turn changed the local relative humidity. After the spin coating, the samples were dried in a vacuum oven for several hours to ensure complete solvent removal.

Atomic Force Microscopy. After each SFA experiment, the polymer surfaces were removed from the apparatus, and both surfaces were imaged by tapping-mode AFM using a MultiMode scanning probe microscope (Veeco/Digital Instruments, Santa Barbara, CA). All images were taken in ambient conditions with a commercial silicon cantilever (NCL Pointprobe type, Nanosensors, Switzerland). Each image was flattened (1st order) and plane-fitted using a 2nd order polynomial before any analysis was done.

Results and Discussion

Force Measurements between Periodically Rough ("Patterned") Surfaces. With the spin casting method described above, polymer surfaces of PS−PVP with varying "island" densities were formed with RMS roughness, σ, in the range from 0.5 to 6.1 nm. Figure 2 shows a representative AFM image

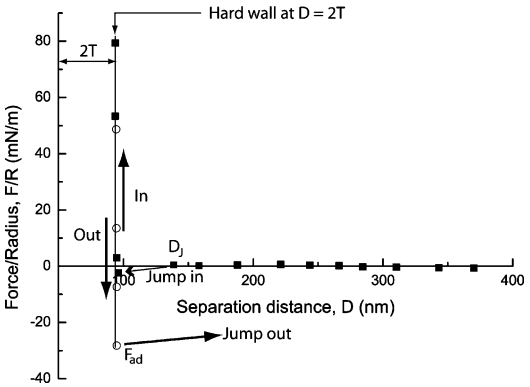

Figure 3. Measured force (normalized by the radius of curvature R) versus distance for the PS−PVP diblock copolymer "patterned" surfaces.

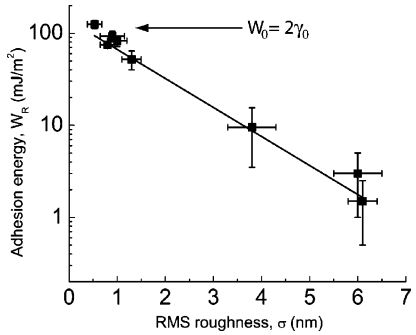

Figure 4. Adhesion energy measurements of two PS−PVP diblock copolymer surfaces as a function of increasing surface roughness. The receding adhesion values, W_R, were calculated from the "pull-off" forces using eq 1 with the value of $R \approx 2$ cm being taken as the macroscopic radius as measured from the FECO fringes.

of a PS−PVP surface for $\sigma = 6$ nm. We may note that both the vertical (height) and lateral (nearest-neighbor center-to-center distance) distributions are nonrandom, both falling within a fairly narrow range of distances.

Force curves were obtained both on compression and separation (Figure 3). These were highly reversible and reproducible, and they behaved similarly to a JKR-type contact for all of the "patterned" diblock polymer surfaces tested, independent of the morphology. Figure 3 shows that as the surfaces approached, they 'jumped' into adhesive contact from a distance D_J of up to 30 nm, as measured between the top of the bumps. At the end of the jump, the surfaces immediately flatten due to adhesion at the "hard-wall" contact separation of $D = 2T$, meaning that the repulsion was very steep, similar to a hard-core repulsion, and located at twice the mean polymer film thickness, T. Additionally, no "structure" or roughness was evident from the FECO fringes, as was often seen with the randomly rough surfaces described below. Instead, the fringes were seen to slightly broaden, i.e., become more diffuse, due to the varying thickness of the heterogeneous polymer−air interface.

From the measured pull-off forces between two PS−PVP surfaces, F_{ad}, the estimated adhesion energies W_R were obtained from eq 1. These are plotted as a function of increasing RMS roughness in Figure 4. The plot shows a sharp exponential decrease in the effective adhesion force F_{ad} (or W_R) from a value close to the thermodynamically expected value at $\sigma = 0$, with a decay length of $\lambda \approx 1.4$ nm. Thus, we find

$$F(\sigma) = (3/2)\pi R W(\sigma) \approx (3/2)\pi R W_0 \, e^{-\sigma/\lambda} \qquad (2)$$

where $W(\sigma) = W_0 \, e^{-\sigma/\lambda}$ is the effective surface energy, and where λ is presumably a function of the polymer material properties such as its stiffness or elastic modulus K, surface energy γ_0, and possibly other as of yet unknown parameters. The decrease in the adhesion energy is likely directly related to the reduced real contact area. From the JKR theory, in general, this decrease will be further diminished through a higher stiffness K, but opposed by a higher W_0. Interestingly, a simple approach using dimensional analysis suggests that $\lambda \propto W_0/K$ because the units of W_0 and K are N/m and N/m^2. Using typical values of $W_0 \approx 0.1$ N/m and K $\approx 10^9$ N/m^2, we obtain $\lambda \approx 10^{-1}/10^9 \approx 10^{-10}$ m ≈ 0.1 nm, which is a little more than an order of magnitude difference from the measured decay length of 1.4 nm.

Friction measurements between the PS−PVP surfaces were done with and without lubricant (refractive index) oil. However, upon initiating sliding, at least one of the polymer surfaces soon became irreversibly damaged, which could be easily seen from the changing shapes of the FECO fringes. It is very likely that these structured pillars interdigitated easily on shearing, each falling into the space between opposite pillars resulting in "ploughing damage". The friction behavior is quite complex and warrants further investigation.

Force Measurements between Randomly Rough Surfaces. A much wider range of randomly rough surfaces could be produced with the P(VDF−TrFE) copolymers, with σ varying from as low as a few nm to a few hundred nm. Figure 5 shows a few examples of the different morphologies that were produced with P(VDF−TrFE).

To determine if these surfaces could be appropriately described by a fractal dimension, a procedure following Persson et al.[2] was performed on the digitized images. Using this analysis, it was determined that these surfaces were not fractal and do not possess a unique fractal dimension or Hurst parameter.[6]

Force−distance data obtained with the P(VDF−TrFE) copolymer surfaces is presented in Figure 6. For surfaces with roughness varying from $\sigma = 3$ to $\sigma = 220$ nm, all normal forces measured on approach after the initial (slightly adhesive) contact exhibited an almost perfect exponential repulsion with decay lengths λ from 2.0 to 40.0 nm. Measurements were done in pure dry air (unlubricated surfaces) as well as with the refractive index liquid oil between the surfaces (lubricated surfaces). It was expected that the lubricated systems would display different short-range force−distance curves compared to the dry, unlubricated surfaces due to the differences in the van der Waals and solvation forces in the two systems. However, the repulsive forces between the dry and lubricated systems were overall very similar, especially for the rougher surfaces where the short-range forces are less important and where the repulsion is dominated by the asperities and their bulk elastic or plastic properties. We show our results for the lubricated surfaces (in oil) because of the increased accuracy of measuring the separation D in these systems, as discussed above.

The repulsive forces measured on separation (unloading) were generally weaker than on approach, especially for the rougher surfaces (see white points in Figure 6A); these retracting forces could not be fitted using an exponential form. However, on second and subsequent approaches, the resulting force curves, both on approach and separation, were very reproducible. A computer simulation[35] using these surfaces with $\sigma = 14.0 \pm 1.0$ nm also found an exponentially repulsive force of magnitude and range similar to what was measured (Figure 7).

Two trends are immediately noticeable from the forces of Figure 6. First, the onset of the repulsive force (first touch of

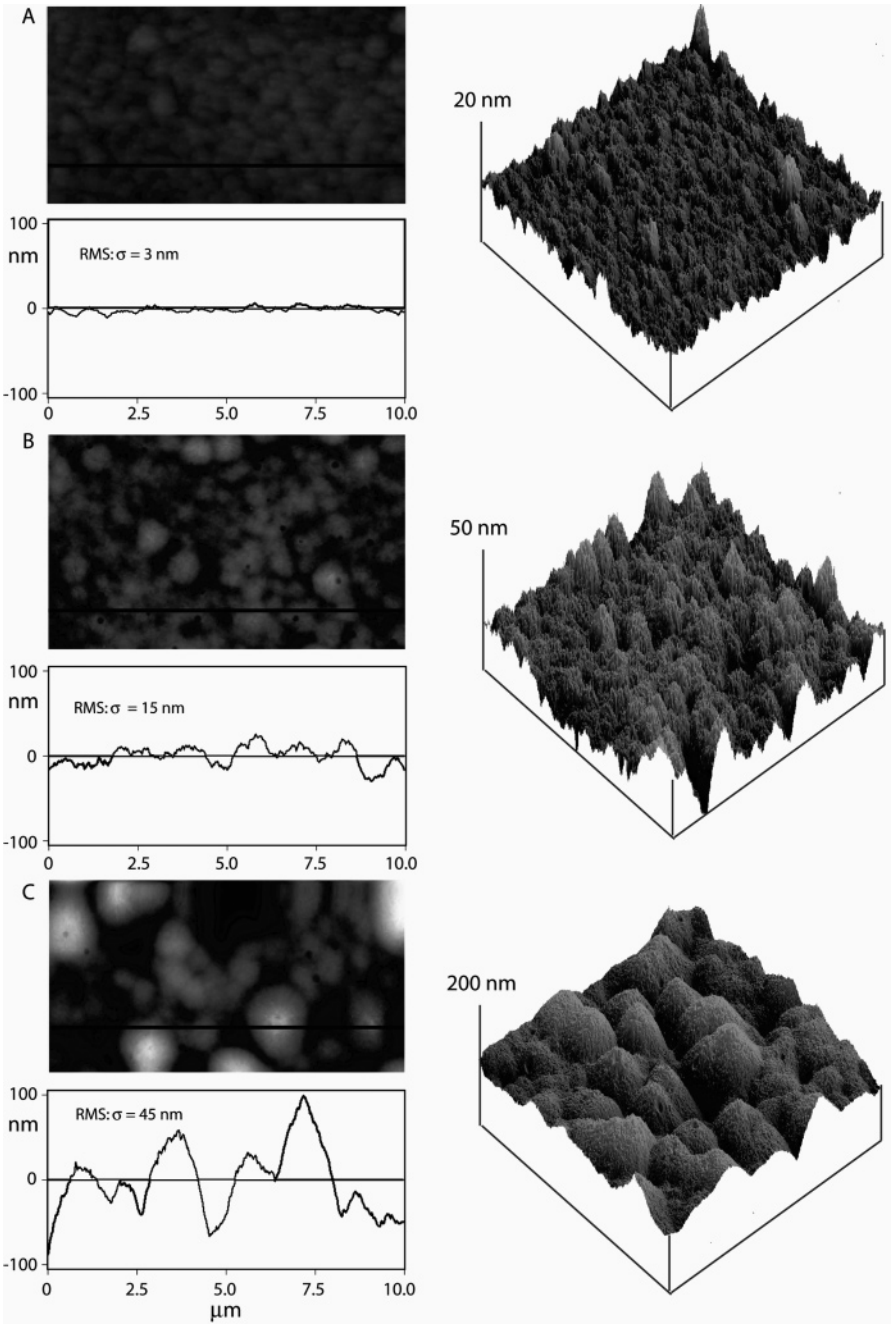

Figure 5. AFM images of three rough P(VDF−TrFE) copolymer surfaces with (A) $\sigma = 3$ nm, (B) $\sigma = 15$ nm, and (C) $\sigma = 45$ nm. Note that these randomly rough surfaces also had a T_g of −28 °C, compared to the T_g of +100 °C of the patterned surfaces.

the outermost asperities) shifts to larger separations as the surfaces get rougher. Second, the exponential decay length λ increases with increasing surface roughness σ (Figure 8). At large and small separations, deviations from the almost perfectly exponential force−distance regimes were often observed. At large separations, the forces were less repulsive due to the attractive short-range van der Waals and/or solvation forces between the initially contacting asperities. At small separations, the forces became more steeply repulsive as the asperities on the two interacting surfaces cannot be compressed any further: a new regime is entered where the fine-grained morphology of the *surface* asperities becomes irrelevant and where the global or coarse-grained (Hertzian) compression and deformation of the *bulk* polymer material takes over, now determined by its bulk elastic modulus. However, we could not clearly distinguish when one regime (local asperity compressions, exponential repulsion) was taken over by the other (global Hertzian compression): even at the highest loads applied, corresponding to $F \approx 30$ mN, $F/R \approx 1500$ mN/m, and $P \approx 12$ MPa, the compression was still in the exponential force regime.

Comparison of the forces for dry and lubricated surfaces (Figure 8) revealed little difference in their exponential force regimes. The addition of the oil caused the repulsion to start 3.5 ± 0.5 nm further out than for the dry unlubricated surfaces, and the decay lengths λ were, on average, higher by 5.0 ± 1.5 nm.

The absence of a detectable exponentially repulsive force regime in the case of the patterned PS−PVP polymeric surfaces (Figure 3) is not surprising. The asperities on these surfaces had the unique characteristic of possessing the same height. This quantized, or terraced, structure dictates that these surfaces should behave as smooth, flat polymer surfaces, albeit with a

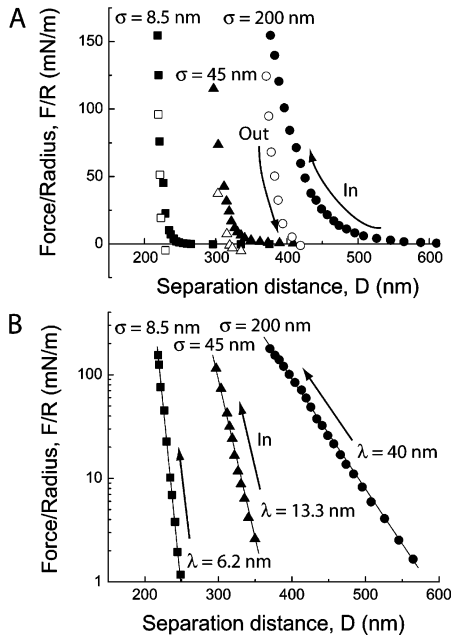

Figure 6. (A) Force−distance measurements of these different rough P(VDF−TrFE) copolymer surfaces in a linear plot. Filled symbols correspond to surfaces on approach (In) and open symbols on separation (Out). (B) Same data on a semilog plot to illustrate the exponentially repulsive force−distance regime.

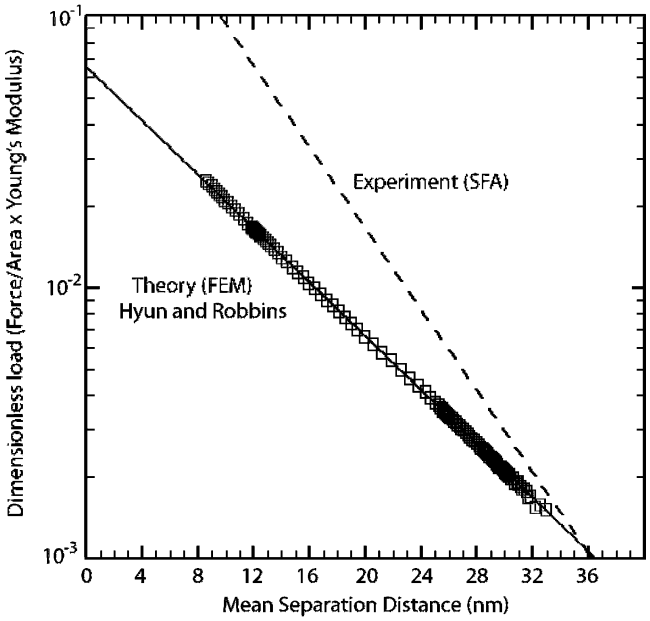

Figure 7. Comparison between finite element calculation for elastic surfaces and experimental result for the repulsive force (made dimensionless) upon compression of two randomly rough surfaces of RMS roughness $\sigma = 14$ nm.

reduced contact area. It is, however, possible that the repulsion was exponential but with an undetectably short decay length ($l < 3$ Å). Even for the surfaces with the largest σ, no exponential curve could be detected within our resolution. Therefore, it may be that random height roughness is a prerequisite for an exponentially repulsive force regime.

Normal Forces between Other Rough Surfaces. The exponential repulsion seen for the randomly rough P(VDF−TrFE) surfaces is expected classically as shown by Greenwood and Williamson.[36] Figure 9 shows examples of previous loading-only force−distance curves measured between four very different types of rough or particle-coated surfaces, both hard and

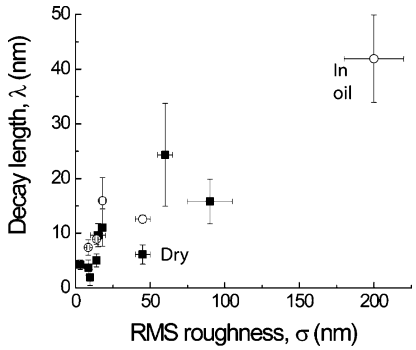

Figure 8. Correlation of the decay length λ (extracted from the exponential force regimes of two compressed P(VDF−TrFE) copolymer surfaces) with the RMS surface roughness. Filled symbols represent decay lengths obtained with dry, unlubricated systems; open symbols are for surfaces immersed in oil.

soft, and conducted in different environments (both in air and liquid).[37] Each of these systems exhibited an exponentially repulsive force regime, with deviations at the beginning of the repulsion (in the case of Figure 9A,B manifested by weakly adhesive contacts determined by the touching of the outermost asperities), and/or at the end of the force curve (in the case of Figure 9C,D manifested by hard walls as $D \rightarrow 0$). Only in the case of (B) was there a final jump into adhesive contact from point *J*. In these earlier experiments, the measured forces were not correlated with the surface roughness, which was not measured, nor were the weak "far-field" adhesive forces measured, as in the present study.

Adhesion Forces between Randomly Rough P(VDF−TrFE) Surfaces. The adhesion energy versus roughness, $W(\sigma)$, for the randomly rough P(VDF−TrFE) system is shown in Figure 10. In contrast to the diblock polymer (Figure 4), the P(VDF−TrFE) copolymer showed no obvious correlation between σ and W. Smooth and rough surfaces exhibited similar adhesion energies ($W_0 \approx 55$ mJ/m^2) when a preload of 20 mN/m was used. It seems that the segmental entanglements of the polymers, which are expected to correlate directly with the *real* contact area,[38] is the major factor for the high adhesion energy.

On separating, small jump-outs, indicative of adhesion between discrete contacts, could be observed. That the adhesion of two rough P(VDF−TrFE) copolymer surfaces is mainly due to segmental interdigitation at the asperity junctions could be shown by comparing the symmetric system to an asymmetric one where a rough P(VDF−TrFE) surface was pressed against a molecularly smooth bare mica surface. This setup, with only one rough polymer surface ($\sigma = 115 \pm 10$ nm) resulted in no adhesion. Furthermore, this was the only system studied that did not lead to any adhesion hysteresis in the JKR plot ($\Delta\gamma = \gamma_R - \gamma_A = 0$). However, the exponential repulsion during compression of the asymmetric setup was still observable. This clearly shows that interfacial interdigitation of polymer chains across the two rough P(VDF−TrFE) copolymer surfaces was responsible for the adhesion hysteresis and increased adhesion on unloading but is irrelevant for the exponential force on loading. On the other hand, JKR measurements of a smooth P(VDF−TrFE) copolymer surface ($\sigma = 15 \pm 5$ nm) against a bare mica surface revealed a small adhesion energy (~20 mJ/m^2) and some hysteresis. The small adhesion is due to the finite real contact area of the polymer with mica on loading to F_{max}.

As a further comparison of the differences between the two polymer systems (PS−PVP, which showed little or no hysteresis, and P(VDF−TrFE), which showed large hysteresis), Figure 11 shows the adhesion energy as a function of the maximum

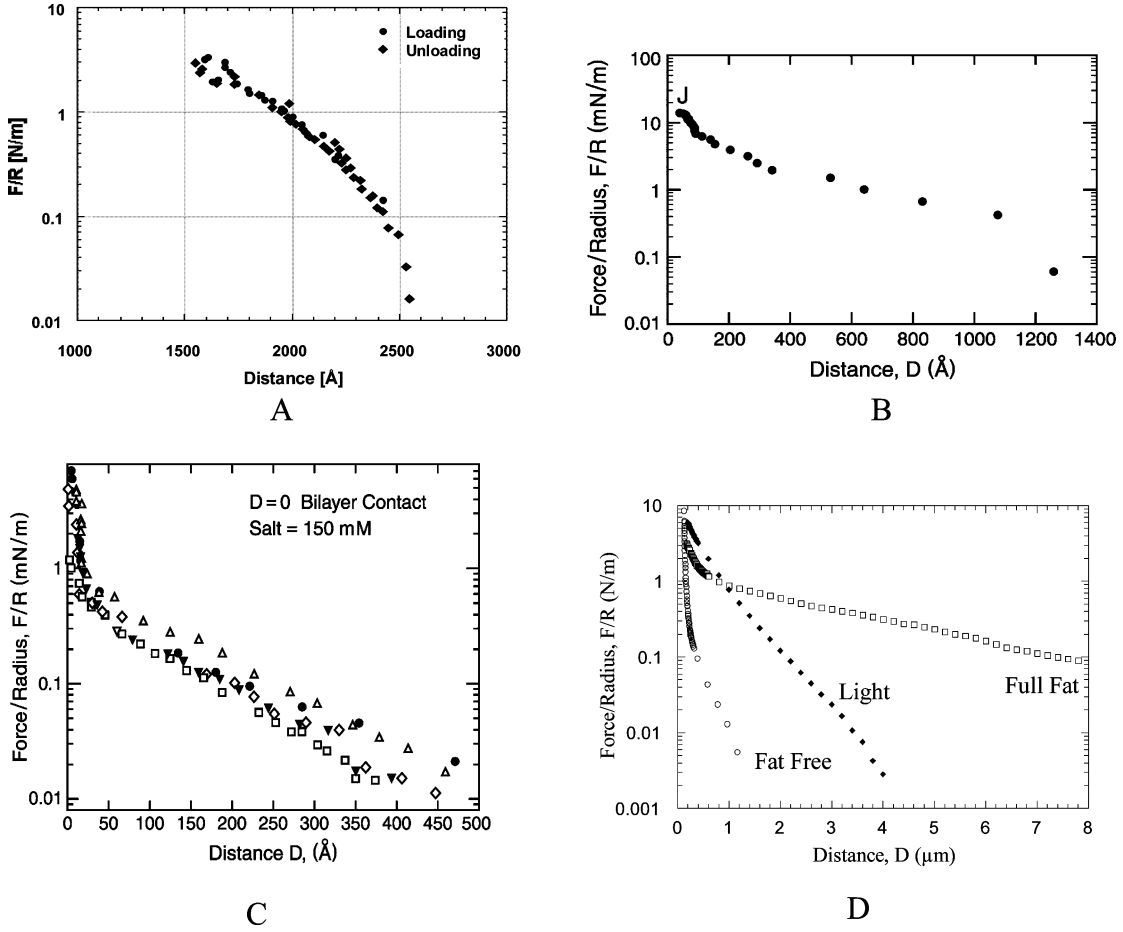

Figure 9. Force−distance measurements for four different systems with different presumed random surface roughness, where each shows an exponentially repulsive force over a significant distance regime. (a) Rough and porous silica surfaces in air. (b) Rough iron oxide surfaces in aqueous solution. (C) Trapped surface-adsorbed DODAB/DOPE surfactant vesicles between two rigidly supported bilayers in 150 mM KNO_3 solution. The white and black symbols indicate compression and separation, respectively. (D) Mica surfaces across an oil-in-water food emulsion (mayonnaise) composed of emulsion droplets and hard aggregated protein particles in water.

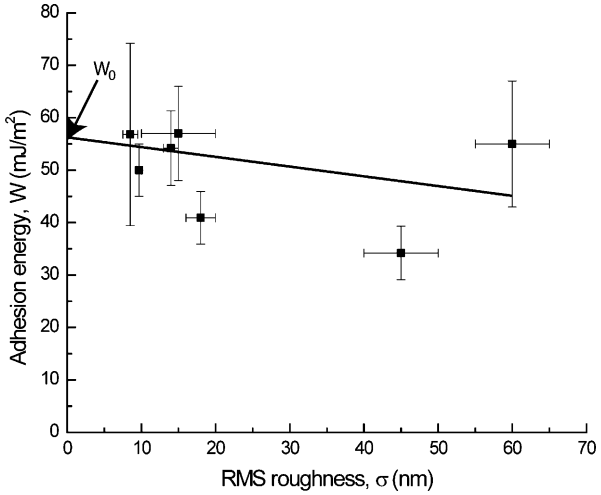

Figure 10. Adhesion of randomly rough P(VDF−TrFE) copolymer surfaces as a function of RMS roughness.

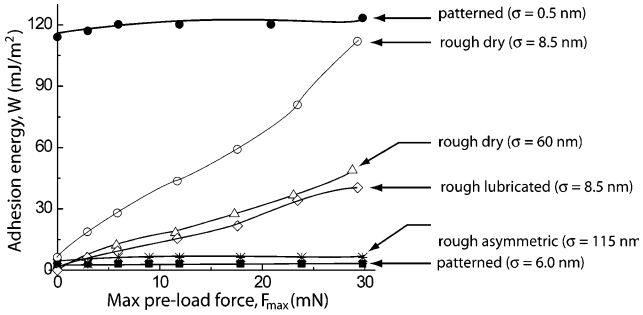

Figure 11. Adhesion energy W as a function of applied normal preload force F_{max}. Filled symbols, ●, ■, represent the patterned PS−PVP diblock copolymer and open symbols, ○, △, ◇, the randomly rough P(VDF−TrFE) copolymer. The diamonds, ◇, represent the same sample as the open circles, ○, but lubricated with the refractive index oil. Points ∗ represent the asymmetric system with a randomly rough P(VDF−TrFE) copolymer surface against bare mica. Note the roughly linear dependence of W against F_{max}.

preload force F_{max} for the two polymers at different surface roughnesses. Only the patterned PS−PVP surfaces showed no dependence on the maximum applied load at any roughness, indicative of no hysteresis and, therefore, no interdigitation of the polymer chains (as previously noted and attributed to its high T_g of 100 °C). Similarly for the asymmetric system of P(VDF−TrFE) against mica where again, but for a different reason, no cross-interfacial interdigitation can occur. In contrast, both smooth and rough P(VDF−TrFE) copolymer surfaces reveal a linear dependence of the adhesion energy on the normal load, F_{max}. This provides further support for the notion that the real contact area of rough surfaces is proportional to F_{max}, as was first concluded by Bowden and Tabor in their classic paper[39] more than 60 years ago in which they measured the electrical resistance of a metal−metal junction as a function of the applied load.

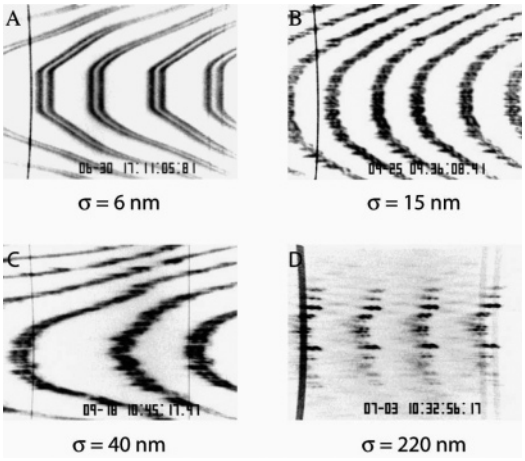

Figure 12. FECO fringes of (A) patterned PS−PVP surfaces (cf. corresponding AFM images in Figure 2) as well as smooth P(VDF−TrFE) surfaces (not shown); and (B)−(D): rough P(VDF−TrFE) surfaces (cf. AFM images in Figure 5). The fringes of the highly rough surfaces (panels B−D) are noticeably nonuniform due to the nonuniform reflectance and scattering of the white light passing orthogonally through the two polymer−air interfaces (cf. Figure 1B).

The adhesion was significantly reduced after the refractive index oil was injected between the two P(VDF−TrFE) copolymer surfaces. As shown in Figure 11, the adhesion−load relationship is still linear but with a smaller slope. It is known that an intervening wetting medium, in this case oil between P(VDF−TrFE), reduces the van der Waals force between two surfaces and, in this case, may also hinder the interdigitation if a thin film of the oil separates the surfaces, either of which could explain the reduced slope. Generally, for both the PS−PVP and P(VDF−TrFE) copolymer systems, both the adhesion energy and the adhesion hysteresis (in the case of P(VDF−TrFE)) decreased after the addition of the oil between the surfaces.

Surface Morphology and Deformations. The rough P(VDF−TrFE) surfaces showed very different FECO fringes from those commonly seen with totally smooth surfaces or those seen with the patterned PS−PVP surfaces (Figure 12). Figure 12B−D shows typical fringe patterns of the P(VDF−TrFE) surfaces at three different roughnesses. As the surfaces become rougher, the fringes become broader and more diffuse (less intense) due to the increased lateral variability in refractive index or thickness (T_1 and T_2 in Figure 2) and scattering (reduced transmittance) of the light. Above a certain roughness, the β and γ components of each FECO fringe can no longer be distinguished.[40] Although the FECO fringes give a faithful replica of the surface cross-sectional topography, the increased nonuniformity of the FECO fringes for increasingly rougher surfaces significantly diminishes the quantitative accuracy of the optical measurements. Thus, the fringes in Figure 12D could not be used for accurate distance or surface-shape measurements anymore. In principle, one can still obtain statistical properties of surface roughness from the fringes,[41] but in this work, AFM was used for this purpose as it has a higher lateral resolution. For very rough surfaces ($\sigma >$ 200 nm), the fringes can be seen clearly only when the surfaces are compressed under a high load ($F >$ 25 mN), corresponding to pressures P in excess of 10 MPa, when the rough surfaces and the fringes become flattened.

The loss of the MBI−FECO technique's accuracy for measuring the separation distance with increasing surface roughness can be dramatically improved by introducing a liquid between the surfaces that has a similar refractive index to that of the surfaces (polymer layers). With the liquid present, the refractive indices are "matched" and no light is scattered; the FECO fringes are sharper and can now be observed with significantly higher accuracy than in air (see Figure 13A,B for two separated surfaces, and C,D for two compressed/flattened surfaces). Additionally, with the intervening liquid, the analysis becomes much more tractable as the system is now a three-layer interferometer[34] of mica−uniform medium−mica as opposed to a quasi-five-layer interferometer (mica−polymer−air−polymer−mica). However, adding a refractive index matching liquid results in losing the ability to visualize the roughness through the FECO fringes.

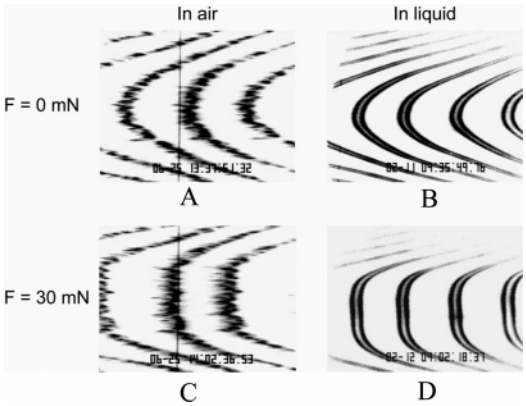

Figure 13. Fringes of two rough P(VDF−TrFE) surfaces of RMS roughness $\sigma = 60$ nm (A) close to contact in air and (B) after injection of liquid that matches the polymer's refractive index. In (B) the fringes appear smooth and uniform, independent of the surface roughness. (C) and (D) are for the same surfaces shown in air and liquid, respectively, but now flattened under a compressive pressure of 15 atm.

As illustrated in Figure 13, in liquid, the fringes always appeared very uniform and smooth, independent of the polymer surface roughness. This indicates that all the local (asperity) deformations occur at the polymer−polymer junctions or interfaces, rather than at the polymer−mica substrate interfaces (cf. Figure 1A). However, this does not diminish the roles that the bulk elastic modulus of the surfaces and the underlying material and glue layers play in addition to the nanoscale roughness and modulus. The former determine the macroscopic/microscopic or global deformations whereas *both* determine the nanoscopic (local asperity) deformations. Thus, the bulk material stiffness determines the global deformation, which in turn affects the local stresses and contact areas. The global deformations, as illustrated in Figure 13D, suggest that the global contact geometry is Hertzian-like, although a full analysis of the fringe shape as a function of load would be necessary to establish the precise "contact mechanics" of such rough surfaces.

Two types of deformations can be distinguished when an initially round, rough polymer surface is pressed against another surface. As illustrated schematically in Figure 1, and quantitatively in Figure 14A, one is the "local" nano- and sub-microscale deformations of the asperities; the other is the "global" or macroscale deformation of the bulk geometry. The latter is captured by the mean shape of the FECO fringes, which was used to measure the projected or "apparent" contact area $A = \pi a^2$. Figure 14A is a schematic of how the contact radius was "seen" and measured as a function of load. Both the polymers used had a similar bulk elastic modulus of $K \approx 1$ GPa, and the bulk stiffnesses of the underlying mica and glue substrates were nearly identical for both systems. Therefore, it is reasonable to assume that the significant differences observed upon compressing the two types of polymer surfaces are largely due to their nanoscale roughness and asperity properties and not to any bulk material property or the global radius R (Figure 1A).

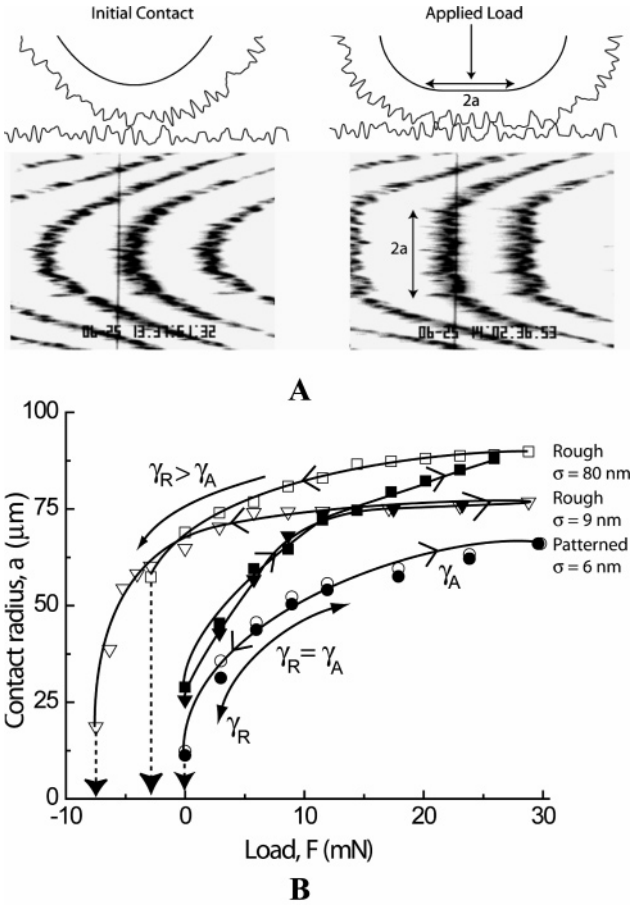

Figure 14. (A) Schematic of rough surfaces at first contact ($F \approx 0$) and under an applied load ($F = 30$ mN) with the respective FECO fringes showing how the contact radius a was determined. (B) "JKR plots" giving the adhesion hysteresis of the patterned PS−PVP and rough P(VDF−TrFE) surfaces. The radius of the contact area a is plotted as a function of the externally applied load F. Squares and triangles correspond to two different rough surfaces and circles are for patterned surfaces for which $\gamma_A = \gamma_R$. White and black symbols are for the loading and unloading paths, respectively.

Figure 14B shows the large hysteresis of P(VDF−TrFE) and its near total absence for the patterned PS−PVP surfaces. The large hysteresis of the rough surfaces indicates that on coming into contact, their surface loops and chain ends of the two P(VDF−TrFE) surfaces interdigitate across the asperity junctions.[38,47] This should not be surprising because the experiments with P(VDF−TrFE) were carried out well above its T_g of −28 °C (compared to +100 °C for PS−PVP). These differences are reflected in the "JKR plots" of Figure 14B, giving the contact radius vs load for the two types of surfaces.

Conclusion

This work is a continuation and a more thorough study of phenomena that have been seen in many of our earlier experiments[20,21,26] on the effects of surface roughness and material stiffness on the adhesion of solids. Normal force−distance measurements on several different *randomly rough* surfaces conducted under different environmental conditions (in air and liquid) all show an extended exponentially repulsive force regime due to the compression of the asperities. The repulsive regime is preceded by a weak attractive (adhesive) regime as the outermost asperities first touch or finally separate (detach). Our results on the decreasing adhesion energy with increasing roughness appear to be consistent with the earlier classic works of Bowden and Tabor,[42] showing that the real contact area is proportional to the applied load, and by Fuller and Tabor[43] and later workers[44,45] on the effects of surface roughness and material stiffness on the adhesion of solids.

But in addition, we find that the repulsive and especially the adhesive regimes depend very much both on the nature of the roughness (not just the RMS) and on the temperature relative to T_g. Thus, for the two polymer systems studied at room temperature ($T = 23$ °C), randomly rough P(VDF−TrFE) copolymer surfaces ($T_g = -28$ °C) and textured or semiordered PS−PVP diblock copolymer surfaces ($T_g = +100$ °C), the adhesion of the former depend strongly on the roughness, but also on the load (or pre-load), and exhibited significant adhesion hysteresis effects. These effects are attributed to the low T_g of P(VDF−TrFE) (lower than the experimental temperature), which on the basis of previous studies[38,46,47] enables the chains to locally interdigitate across the asperity junctions, resulting in an increase in the real contact area (and/or number of van der Waals bonds) and adhesion with time. The exponentially repulsive steric force−distance regime occurs regardless of whether one or both surfaces are rough and, for the symmetrical system, was well-described by a finite element simulation (Figure 7).

In contrast, the second type of rough but "patterned" or "semiordered" polymer surface, the diblock copolymer PS−PVP, ($T < T_g = 100$ °C), exhibited a very steep, almost hard wall repulsive force regime whose functional form was consequently difficult to determine. Additionally, the patterned surfaces exhibited no load effects on their adhesion, nor any adhesion hysteresis. This is attributed to the high stiffness and T_g of PS−PVP, which prevented any interdigitation of their segments on coming into contact.

Our main conclusion may therefore be summarized by saying that depending on the nature of the roughness but also the load, T_g and time (or loading/unloading rate), some polymer surfaces may exhibit a roughness-dependent adhesion but a sharp roughness-independent repulsive regime, whereas others, having the same RMS roughness, may exhibit an adhesion that is largely independent of the roughness but a broad exponentially repulsive force regime closer in.

The observation of an extensive exponential repulsion has important implications for tribology, colloid science, powder technology, and materials science. For example, the density or volume of granular materials has long been known to have a logarithmic dependence on the externally applied isotropic pressure or stress, as found, for example, in the compaction stage during the processing of ceramic materials.[48] This particular observation has been modeled in many different ways but none have managed to satisfactorily explain this phenomenon. Our apparently universal exponential repulsion upon compressing randomly rough surfaces, whether elastic or anelastic (elasto-plastic), may be the general underlying reason for this effect. Recent work on the confinement of nanoparticles have also indicated an exponential force upon compression, suggesting that this relationship could be prevalent among quite different types of heterogeneous surfaces.[49]

It should also be interesting to correlate the surface roughness of random and patterned surfaces with their friction forces. The polymers used in this study were found to be unsuited for friction experiments; even at low loads, there was irreversible wear and ploughing damage due to failure at the polymer−mica interface.

Acknowledgment. This work was funded by the Department of Energy under Grant Number DE-FG02-87ER45331. M.B.

was partially funded by a postdoctoral grant from the Swiss National Science Foundation. We thank S. Hyun and M. Robbins for their FEM analysis and for preparing Figure 7. We are also grateful to D. McLaren for preparing Figure 1 and to R. Segalman for synthesizing the block copolymer (PS-P2VP) used in this study.

References and Notes

(1) Johnson, K. L. *Contact Mechanics*; Cambridge University Press: Cambridge, 1985.
(2) Persson, B. N. J.; Albohr, O.; Tartaglino, U.; Volokitin, A. I.; Tosatti, E. *J. Phys.: Condens. Matter* **2005**, *17*, R1−R62.
(3) Geminard, J. C.; Losert, W.; Gollub, J. P. *Phys. Rev. E: Stat. Phys., Plasmas, Fluids, Relat. Interdiscip. Top.* **1999**, *59*, 5881−5890.
(4) Yu, C. M.; Tichy, J. *Tribol. Trans.* **1996**, *39*, 537−546.
(5) Thomas, T. R. *Rough Surfaces*, 2nd ed.; 1999.
(6) Zhao, Y.; Wang, G.-C.; Lu, T.-M. *Characterization of Amorphous and Crystalline Rough Surface: Principle and Applications*; 2001.
(7) Bhushan, B.; Koinkar, V. N. *Sensor Actuators, A* **1996**, *57*, 91−102.
(8) De Boer, M. P.; Knapp, J. A.; Michalske, T. A.; Srinivasan, U.; Maboudian, R. *Acta Mater.* **2000**, *48*, 4531−4541.
(9) Azarian, M. H.; Bauer, C. L.; O'Connor, T. M.; Crone, R. M.; Jhon, M. S. *Tribol. Trans.* **1993**, *36*, 525−534.
(10) Suh, A. Y.; Polycarpou, A. A. *Tribol. Lett.* **2003**, *15*, 365−376.
(11) Israelachvili, J.; Maeda, N.; Rosenberg, K. J.; Akbulut, M. *J. Mater. Res.* **2005**, *20*, 1952−1972.
(12) Gao, J. P.; Luedtke, W. D.; Landman, U. *Tribol. Lett.* **2000**, *9*, 3−13.
(13) Luan, B. Q.; Robbins, M. O. *Nature* **2005**, *435*, 929−932.
(14) Rabinovich, Y. I.; Adler, J. J.; Ata, A.; Singh, R. K.; Moudgil, B. M. *J. Colloid Interface Sci.* **2000**, *232*, 17−24.
(15) Beach, E. R.; Tormoen, G. W.; Drelich, J.; Han, R. *J. Colloid Interface Sci.* **2002**, *247*, 84−99.
(16) Quon, R. A.; Knarr, R. F.; Vanderlick, T. K. *J. Phys. Chem. B* **1999**, *103*, 5320−5327.
(17) Knarr, R. F.; Quon, R. A.; Vanderlick, T. K. *Langmuir* **1998**, *14*, 6414−6418.
(18) Alcantar, N. A.; Park, C.; Pan, J. M.; Israelachvili, J. N. *Acta Mater.* **2003**, *51*, 31−47.
(19) Kim, H. C.; Russell, T. P. *J. Polym. Sci. Pol. Phys.* **2001**, *39*, 1848−1854.
(20) Luengo, G.; Tsuchiya, M.; Heuberger, M.; Israelachvili, J. *J. Food Sci.* **1997**, *62*, 767−812.
(21) Giasson, S.; Israelachvili, J.; Yoshizawa, H. *J. Food Sci.* **1997**, *62*, 640−652.
(22) Golan, Y.; Drummond, C.; Homyonfer, M.; Feldman, Y.; Tenne, R.; Israelachvili, J. *Adv. Mater.* **1999**, *11*, 934−937.
(23) Israelachvili, J. N.; McGuiggan, P. M. *J. Mater. Res.* **1990**, *5*, 2223−2231.
(24) Israelachvili, J. N.; Adams, G. E. *J. Chem. Soc., Faraday Trans. I* **1978**, *74*, 975−1001.
(25) Israelachvili, J. *Intermolecular and Surface Forces*; Academic Press: London, 1991.
(26) Horn, R. G.; Israelachvili, J. N.; Pribac, F. *J. Colloid Interface Sci.* **1987**, *115*, 480−492.
(27) Johnson, K. L.; Kendall, K.; Roberts, A. D. *Proc. R. Soc. London, Ser. A* **1971**, *324*, 301−313.
(28) Chen, Y. L.; Helm, C. A.; Israelachvili, J. N. *Langmuir* **1991**, *7*, 2694−2699.
(29) Segalman, R. A.; Schaefer, K. E.; Fredrickson, G. H.; Kramer, E. J.; Magonov, S. *Macromolecules* **2003**, *36*, 4498−4506.
(30) Yokoyama, H.; Mates, T. E.; Kramer, E. J. *Macromolecules* **2000**, *33*, 1888−1898.
(31) Benz, M.; Euler, W. B.; Gregory, O. J. *Langmuir* **2001**, *17*, 239−243.
(32) Benz, M.; Euler, W. B.; Gregory, O. J. *Macromolecules* **2002**, *35*, 2682−2688.
(33) Benz, M.; Euler, W. B. *J. Appl. Polym. Sci.* **2003**, *89*, 1093−1100.
(34) Tadmor, R.; Chen, N. H.; Israelachvili, J. N. *J. Colloid Interface Sci.* **2003**, *264*, 548−553.
(35) Pei, L.; Hyun, S.; Molinari, J. F.; Robbins, M. O. *J. Mech. Phys. Solids* **2005**, *53*, 2385−2407.
(36) Greenwood, J. A.; Williams, J. B. *Proc. R. Soc. London, Ser. A* **1966**, *295*, 300−319.
(37) Israelachvili, J.; Giasson, S.; Kuhl, T.; Drummond, C.; Berman, A.; Luengo, G.; Pan, J. M.; Heuberger, M.; Ducker, W.; Alcantar, N. A. *Proc. Leeds−Lyon Symp. Tribol. 26th* **2000**, *38*, 3−12.
(38) Chen, N. H.; Maeda, N.; Tirrell, M.; Israelachvili, J. *Macromolecules* **2005**, *38*, 3491−3503.
(39) Bowden, F. P.; Tabor, D. *Proc. R. Soc. London, Ser. A* **1939**, *169*, 391−413.
(40) Smooth surfaces visualized with the MBI−FECO technique show a distinct fringe doublet due to the birefringence of mica, as seen in Figures 12A, 13B, and 13D.
(41) Bennett, J. M. *Appl. Opt.* **1976**, *15*, 2705−2721.
(42) Bowden, F. P.; Tabor, D. *An Introduction to Tribology*; Anchor Press/Doubleday, 1973.
(43) Fuller, K. N. G.; Tabor, D. *Proc. R. Soc. London, Ser. A* **1975**, *345*, 327−342.
(44) Persson, B. N. J. *Phys. Rev. Lett.* **2001**, *87*, 116101.
(45) Hyun, S.; Pei, L.; Molinari, J. F.; Robbins, M. O. *Phys. Rev. E: Stat. Phys., Plasmas, Fluids, Relat. Interdiscip. Top.* **2004**, *70*, 026117.
(46) Luengo, G.; Pan, J. M.; Heuberger, M.; Israelachvili, J. *Langmuir* **1998**, *14*, 3873−3881.
(47) Maeda, N.; Chen, N. H.; Tirrell, M.; Israelachvili, J. *Science* **2002**, *297*, 379−382.
(48) Stanley-Wood, N. G., Ed. *Enlargement and Compaction of Particulate Solids*, 1983.
(49) Alig, A. R. G.; Akbulut, M.; Israelachvili, J. *Adv. Funct. Mater.* **2005**, submitted.